Observation of surface-state transport in ultrathin Sb

S. Cairns, N. Teasdale, J. Keay, C. K. Gaspe, K. S. Wickramasinghe, T. D. Mishima, M. B. Santos, and S. Q. Murphy[*]

Homer L. Dodge Department of Physics and Astronomy, University of Oklahoma, Norman, Oklahoma 73019, USA

We report magnetotransport studies of ultrathin Sb films. Sb has been identified as a topologically nontrivial element; as a semimetal, however, the interior states dominate the transport in bulk samples. In the ultrathin films studied here, quantum confinement suppresses the interior transport such that surface transport accounts for about 15% of the conduction in 10-bilayer-thick Sb structures. For thicknesses between 5 and 16 bilayers, the conduction increases linearly with film thickness, extrapolating to a *finite* remnant conductivity at zero film thickness. Weak antilocalization (WAL) is observed at low magnetic fields with thickness independent values of the phase breaking length and prefactor (α) implying surface transport coupled to residual interior conduction. At high fields we see an evolution of the magnetoresistance (MR) field dependence from parabolic to sublinear as a function of film thickness. The data are reproduced by a simple model combining parallel parabolic MR from the interior and WAL from the surface.

PACS number(s): 73.50.Jt, 72.20.My, 73.20.Fz

I. INTRODUCTION

The advent of topological phases of matter has brought topology to the forefront of condensed matter physics research. Topological insulators with their insulating interiors and conducting boundaries have spawned a flurry of theoretical and experimental work. This effort has been motivated in part by the symmetry protection afforded to the helical boundary states which leaves them immune to Anderson localization and makes them possible candidates in applications related to spintronics, interconnects, and quantum computing. In a reversal of the usual order, theoretical work by Fu and Kane [1] in 2007 predicted that $Bi_{1-x}Sb_x$, a semiconducting alloy, would be a three-dimensional (3D) topological insulator (TI). The parent solids, Bi and Sb, are both group V semimetals with strong spin-orbit coupling, however, for Sb concentrations between 7% and 22% the alloy is semiconducting [2]. The topological character of the alloy arises from Sb, which possesses a nontrivial topology for the valence band.

Subsequent angle-resolved photoemission spectroscopy (ARPES) experiments by Hsieh *et al.* [3] confirmed the topology of both BiSb and bulk Sb. Scanning probe microscopy of the bulk Sb(111) surface by Seo *et al.* [4] discovered a high transmission rate of the surface states across step edges which was attributed to suppressed backscattering. Gomes *et al.* used scanning tunneling microscopy (STM) and ARPES to image coherent quantum interference attributed to Dirac fermions on a clean Sb(111) surface [5]. Nevertheless, the semimetallic band gap (-180 meV) precluded bulk Sb from being a 3D TI. Since then numerous other materials have been identified as 3D TIs [6]. The majority, however, suffer from bulk transport due to unintentional doping by defects, thus complicating experiments to probe the transport of the symmetry protected surface states. Surprisingly, it is HgTe, an otherwise bulk semimetal, which has demonstrated some of the cleanest surface-state-dominated transport [7] when grown epitaxially on lattice mismatched CdTe, as the induced strain has the effect of opening a heavy/light hole gap. We employ a related approach in which the band gap of semimetallic Sb is opened via quantum confinement in ultrathin layers.

Ultrathin Sb, as an elemental TI [8], offers several potential advantages: It provides a simplified stoichiometry that may lessen the formation of defects; Sb is already included in many III-V molecular beam epitaxy (MBE) chambers, permitting widespread access; and it is compatible with several semiconductor materials and their device processing, allowing for the development of hybrid systems. Thin film Sb also offers a potentially rich phase diagram with band structure calculations predicting a series of quantum phase transitions from topological semimetal to 3D TI to two-dimensional (2D) TI to a conventional insulator as the film thickness is reduced [9]. Moreover, bulk Sb becomes a superconductor under modest pressures, presenting a possible route to topological superconductivity [10].

Sb crystallizes in the $A7$ rhombohedral structure with a two-atom basis. Along $\langle 111 \rangle$ the crystal assembles in bilayers (BLs), stacking in an ABC repeat with a spacing of 0.36 nm per BL. Various calculations [9,11–13] are in agreement that confinement opens the bulk gap for films below 20 BLs, inducing a transition to a 3D TI. A TI state is maintained in freestanding films down to 4–6 BLs, after which the film transitions to a conventional insulator due to hybridization between the boundary states. In one of the few experimental reports on thin film Sb, ARPES measurements by Bian *et al.* [12] showed that even for films as thin as 4 BLs, the expected opening of the surface-state gap did not occur. This was attributed to the suppression of quantum tunneling by interfacial bonds between the film and substrates which preserved the TI phase [12,14].

II. EXPERIMENT

For this study, ultrathin Sb films were grown via molecular beam epitaxy on GaSb(111)A substrates with a lattice mismatch less than 0.1%. The Sb was deposited at a rate of 0.18 nm/s on a 0.5 μm GaSb buffer layer at a low substrate temperature ($\sim$180 °C), during which streaky reflection high energy electron diffraction (RHEED) patterns were observed [15]. Postgrowth images from scanning electron

*smurphy@ou.edu

microscopy on 3.6 and 4 nm thick layers revealed continuous films with smooth terraces extending over distances of 200 nm. Transport studies focused on wafers with a nominal Sb layer thickness from 1 to 6 nm (the majority with a 5 nm GaSb cap). Samples were prepared for measurements in both van der Pauw (several mm square) and Hall (40 μm wide) configurations using conventional photolithography and unannealed pressed/evaporated In for ohmic contacts. Measurements were made on all samples down to 20 K and with some selected samples to ^{3}He and dilution refrigerator temperatures in perpendicular and tilted fields up to 18 T using standard lock-in techniques.

III. RESULTS AND DISCUSSION

All the Sb films displayed resistances that increased with decreasing temperature (see the inset to Fig. 1), in contrast to the metallic ($\frac{dR}{dT} > 0$) behavior of thicker Sb layers grown for deposition rate calibrations. Figure 1 displays the sheet conductivity at 20 K for 17 films as a function of thickness; all films were less conductive than the bulk value extrapolated to equivalent thicknesses, demonstrating suppression of the bulk conduction. As expected, a decrease in the conductivity was observed of the three uncapped samples (open triangles) relative to capped samples of comparable thickness due to an expected reduction in the effective thickness by surface oxidation. For films between 5 and 16 BLs, the conductivity grew linearly with film thickness. The linear behavior may originate from residual bulk conductivity and/or adjustments of the surface bands with thickness, as previously observed in band structure calculations. Below 1.8 nm (5 BLs), the

FIG. 2. (Color online) Longitudinal resistance R$_{xx}$ vs magnetic field in tilted field geometry for a 5.8 nm film at 25 mK. The inset shows the resistance collapsed onto a single curve when plotted vs a perpendicular field.

conductivity showed an abrupt drop, beyond which the conductivity was comparable to three control samples (growth stack without Sb film). The drop, while coincident with theoretical predictions for the transition between the TI and trivial insulator state, is likely due to a percolation transition from incomplete coverage of the Sb film at these low film thicknesses. Notably, the conductivity above this transition extrapolated to a small but *finite* remnant conductivity at zero thickness, as expected for surface transport. The ratio of the conductance at the intercept to the conductance at 3.6 nm suggests that ~15% of the conductivity originates from the surfaces of the 3.6 nm film.

Additional supporting evidence for two-dimensional (2D) transport is revealed in the magnetoresistance (MR) in tilted fields. All of the traces for a given film collapse onto a common curve when plotted as a function of perpendicular field (Fig. 2), indicating the 2D character of the current carrying states. We do caution that because the magnetic length [$l_B = \sqrt{h/eB}$, $l_B(18\text{ T}) = 6$ nm] is larger than the thickest film studied, the perpendicular field dependence excludes 3D transport, but cannot discriminate between a surface state and bulk 2D subbands.

At low fields, positive MR is observed, a signature of weak antilocalization (WAL) and an expected behavior for TI states with their inherent backscattering suppression. The low-field MR was analyzed using the Hikami-Larkin-Nagaoka (HLN) model [16] for WAL in the limit of infinite spin-orbit coupling (i.e., fully suppressed backscattering),

$$\Delta\sigma = -\alpha\frac{e^2}{2\pi^2\hbar}\left[\psi\left(\frac{1}{2} + \frac{H_\phi}{B}\right) - \ln\left(\frac{H_\phi}{B}\right)\right], \quad (1)$$

where ψ is the digamma function and the two free fitting parameters are α, with the expected value of $\frac{1}{2}$ per 2D channel, and H_ϕ, related to L_ϕ, the phase breaking length, by $L_\phi = [\hbar/4eH_\phi]^{\frac{1}{2}}$. Figure 3(b) shows the fit of the HLN model to the data for the 2.3 nm sample at 4 K. The agreement between the model and the data is very good and is representative of that for all the Sb films. WAL was studied
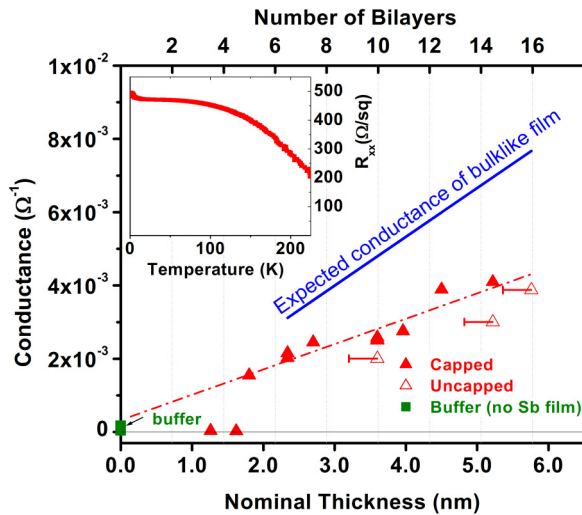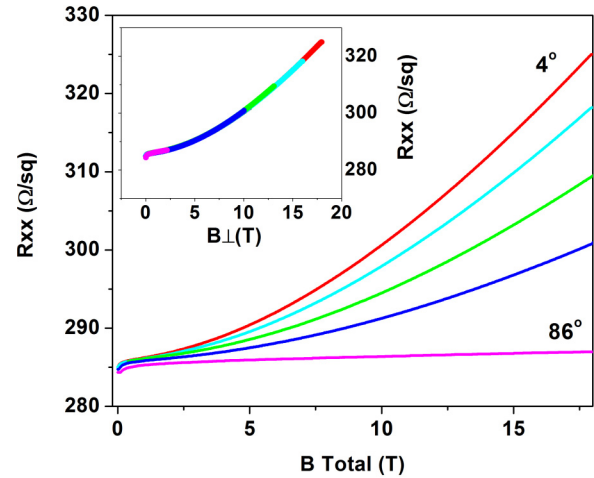

FIG. 1. (Color online) Conductance at 20 K vs film thickness. Samples were grown with either a 5 nm cap of GaSb (solid triangles) or left uncapped (open triangles), with delimiters indicating the reduced effective thicknesses induced by oxidation. Squares represent MBE structures grown without the inclusion of the Sb film. The dashed line shows the linear trend of the conductivity extrapolating to nonzero intercept at zero thickness. The solid blue line shows estimated bulk conductance evaluated for a fully conducting 3D slab. The inset shows the temperature dependence of the resistivity for a 2 nm film.
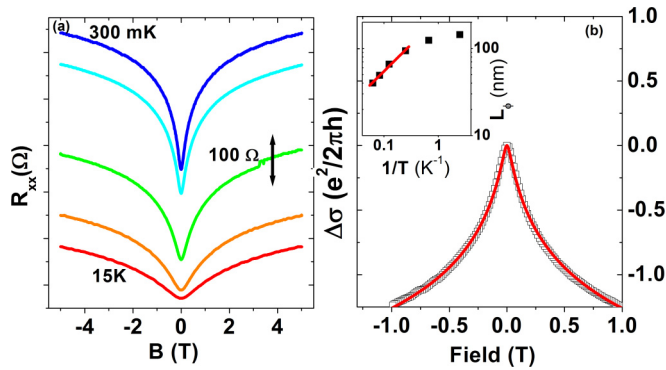
FIG. 3. (Color online) (a) Temperature dependence of the WAL signal from 300 mK to 15 K for a 1.8 nm film (curves displaced for clarity). (b) The conductivity correction at low magnetic fields showing WAL behavior for the 2.3 nm film at 4 K. The solid line is the HLN fit, with the quality of the fit representative for all samples. The inset displays the temperature dependence of the phase breaking length L_ϕ vs $1/T$.

over the range of temperatures from 0.3 to 15 K for the majority of film thicknesses. Extracted values of α proved temperature independent, while L_ϕ [see the inset to Fig. 3(b)] varied with $\sim T^{-1/2}$, consistent with dephasing via 2D electron-electron scattering [17] before saturating at low temperatures. The extracted fitting parameters as a function of film thickness for the capped samples are summarized in Fig. 4 in which the values of α and L_ϕ (at 300 mK) appear relatively thickness independent. As is the case for many WAL measurements in TIs [18–24], we observe $\alpha = 0.5$, which is attributed to residual bulk conduction coupling the two surface channels.

In contrast, the high-field MR shows considerable thickness dependence. This evolution is displayed in the left panel of Fig. 5, where the MR for the samples, normalized to their resistance at zero field, is plotted for a series of different thicknesses. The high-field behavior ($B > 4$ T) progresses from quadratic to linear to sublinear field dependence as the film thickness is reduced. A similar trend as a function of film thickness has been reported for Bi_2Se_3 layers ranging from two to eight quintuple layers [20,21,25,26]. The linear magnetoresistance (LMR) observed in some TI materials
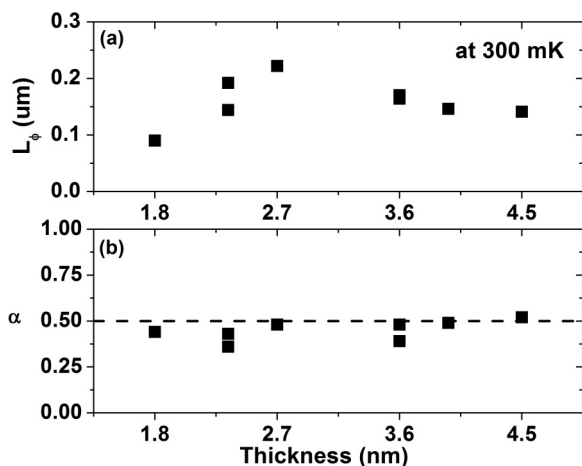
has generated significant attention, since LMR can arise in both conventional quadratically dispersing materials and from Dirac-like linear dispersion.

Parish [27] and Buttiker [28] have considered LMR arising from models based on quadratic band structures in the presence of sample disorder and variations in sample thickness, respectively. Parish *et al.* performed a numerical analysis of an infinite random resistor network, showing that spatial conductivity fluctuations can mix longitudinal and Hall contributions in such a manner that the overall MR is still symmetric with field, but is dominated by a linear term which scales with the width of the mobility disorder. Quantitative comparisons to our data are challenging due to the numerical nature of their work, however, we note that the model was developed to address the sizable (200%) MR observed in silver chalcogenides which dwarfs the more modest MR observed in the Sb films.

Over a decade earlier Büttiker [28] attributed the LMR observed in simple metals to variations in sample thickness (grooves and projections across the current path). An important caveat, however, is that a projection or groove that does not cross the entire current path makes no contribution at all; while our scanning electron microscope (SEM) images show terraces which are continuous across the 4.5 μm image field, it is a considerable extrapolation to expect these terraces to continue across the macroscopic ($\sim$4 mm) sample dimensions of the experimental samples.

An alternative explanation for LMR which invokes a linear dispersion comes from Wang and Lei [29], whose model requires overlapping Landau levels arising from disorder broadening, high temperatures, and/or low fields; however, the sign of the LMR is derived from the g factor which would predict a negative MR for Sb at high fields.

We have employed a straightforward model with bulk and surface channels acting in concert to explain the thickness evolution of the high-field MR. A related model was employed by Assaf *et al.* [30] to explain the temperature evolution of the high-field MR of a Bi_2Te_2Se film. The contribution of the surface channel is taken to be thickness independent, i.e., a fixed surface resistivity ρ_S governed only by the field dependence of the quantum correction, related to parameters α and L_ϕ. The model assumes that the bulk contribution to the MR follows the standard MR, i.e., $R_B(1 + \mu^2 B^2)$, where R_B and μ are the thickness dependent sheet resistance and mobility of the bulk channel.

Adding the two contributions in parallel generates a model with five parameters: α, ρ_S, L_ϕ, R_B, and μ. α is fixed at a value of $\frac{1}{2}$, while the remaining two surface parameters are independently determined by the remnant conductivity at zero thickness from Fig. 1 ($\rho_S \sim 1400$ Ω) and the HLN fits at 300 mK ($L_\phi \sim 180$ nm). Initial values of R_B and μ are chosen for agreement with the measured zero field resistance and magnetoresistance of the 5.8 nm film (quadratic regime). To simulate the observed MR evolution for thinner films, R_B is monotonically increased (from 400 to 8000 Ω), in agreement with the expected effects of increased quantum confinement, while μ is steadily decreased (from 250 to 50 $cm^2/V\,s$), as expected from the enhanced role of interface roughness for thinner channels [31].

FIG. 4. (a) L_ϕ at 300 mK and (b) WAL prefactor α vs Sb thickness for capped samples.
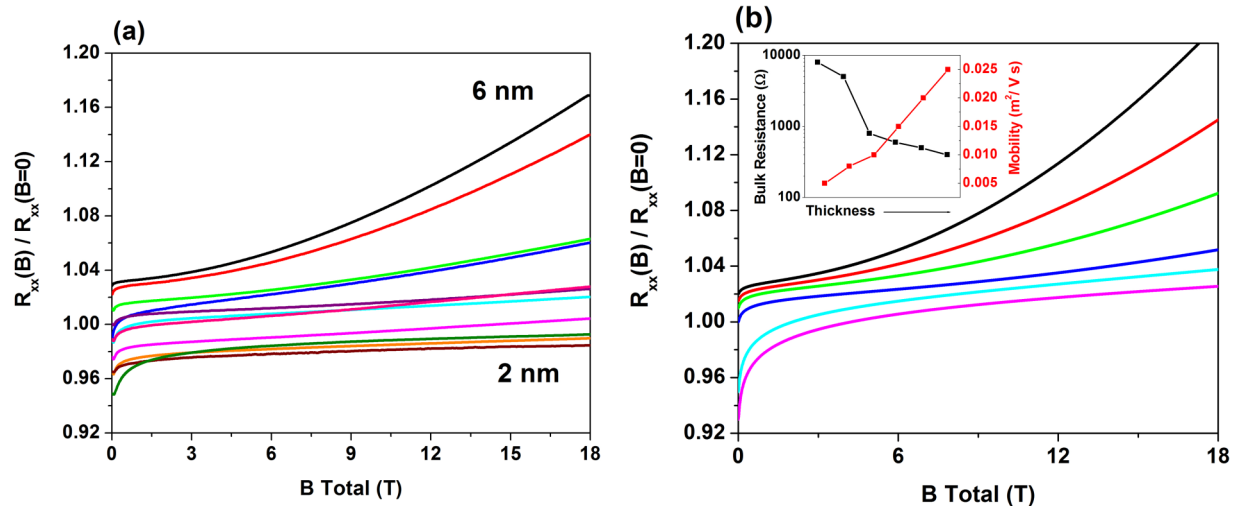
FIG. 5. (Color online) (a) Magnetoresistance measured at 300 mK normalized to zero field value vs total field. Traces are displaced for clarity scaled by relative thickness. The high-field magnetoresistance ($B > 4$ T) shows an evolution from parabolic to linear to sublinear field dependence for decreasing film thickness (6 to 2 nm). (b) Traces generated from the model combining in parallel the bulk MR behavior and surface WAL. The inset gives the values of R_B and μ as a function of film thickness (arb. units). See text for other model details.

The model generated MR traces, with parameters constrained by experiment, are shown in Fig. 5(b) and are an excellent reproduction of the experimental results. While stringent application of the HLN model should limit the simulation to fields of a few tesla where the magnetic length is greater than the mean free path ($\approx$10–20 nm), we allow the model to span the entire experimental range. Despite the lack of an explicitly linear term, the model can generate quasilinear MR in an intermediate regime, suggesting that some of the previously reported LMR in TIs may also arise from this bulk/surface competition [30].

Thus far experimental determinations of the surface carrier densities in these Sb films are indeterminate. A close examination of the electronic dispersion for the thin films reveals the complication: the coexistence of a single Dirac-like surface electron pocket centered about the Γ point *and* six holelike surface pockets lying along the Γ-M direction [3,9]. The experimental Hall slopes (positive, shallow, and linear to 18 T) are consistent with the coexistence of comparable occupation of electron and hole states, but the parameters are not sufficiently well constrained by fits to the Hall and longitudinal resistance. Instead, carrier densities are estimated from band structure calculations ($n_{p,s} \approx$ 2–5 $\times 10^{12}$ cm^{-2}) and yield sample mobilities in the range of 800–2000 cm^2/V s.

IV. SUMMARY

Taken in concert, the finite remnant conductivity, perpendicular field dependence of the MR, and thickness independent WAL parameters all point to surface conductivity in a background of residual bulk. That interpretation is confirmed by a simple parallel surface/bulk model which accurately reproduces the evolution of the high-field MR as a function of film thickness. The observation of remnant surface conduction for films between 5 and 16 BLs is in good agreement with previous ARPES studies. For films below 5 BLs there is an abrupt change in conduction which is likely associated with incomplete coverage of the Sb films, but is coincident with a predicted transition from a topological to a conventional insulator [9,11,12]. Unambiguous evidence of topological transport, however, awaits confirmation of a nontrivial Berry's phase.

In conclusion, we have grown epitaxially smooth Sb quantum films on GaSb via MBE for which the conduction of the semimetallic bulk states is suppressed by quantum confinement, revealing the transport by surface states. The compatibility of and extensive use of Sb in III-V MBE growth bodes well for future efforts to design hybrid devices exploiting the topological transport of the Sb and well-established fabrication and physics of 2D electronic systems.

[1] L. Fu and C. L. Kane, Phys. Rev. B **76**, 045302 (2007).

[2] A. Ibrahim and D. Thompson, Mater. Chem. Phys. **12**, 29 (1985).

[3] D. Hsieh, Y. Xia, L. Wray, D. Qian, A. Pal, J. H. Dil, J. Osterwalder, F. Meier, G. Bihlmayer, C. L. Kane, Y. S. Hor, R. J. Cava, and M. Z. Hasan, Science **323**, 919 (2009).

[4] J. Seo, P. Roushan, H. Beidenkopf, Y. S. Hor, R. J. Cava, and A. Yazdani, Nature (London) **466**, 343 (2010).

[5] K. K. Gomes, W. Ko, W. Mar, Y. Chen, Z.-X. Shen, and H. C. Manoharan, arXiv:0909.0921.

[6] Y. Ando, J. Phys. Soc. Jpn. **82**, 102001 (2013).

[7] C. Brüne, C. X. Liu, E. G. Novik, E. M. Hankiewicz, H. Buhmann, Y. L. Chen, X. L. Qi, Z. X. Shen, S. C. Zhang, and L. W. Molenkamp, Phys. Rev. Lett. **106**, 126803 (2011).

[8] It has also been shown that bismuth is an elemental TI [32].

[9] P. F. Zhang, Z. Liu, W. Duan, F. Liu, and J. Wu, Phys. Rev. B **85**, 201410 (2012).

[10] J. Wittig, J. Phys. Chem. Solids **30**, 1407 (1969).

[11] A. Narayan, I. Rungger, and S. Sanvito, Phys. Rev. B **86**, 201402 (2012).

[12] G. Bian, X. Wang, Y. Liu, T. Miller, and T.-C. Chiang, Phys. Rev. Lett. **108**, 176401 (2012).

[13] S.-X. Wang, P. Zhang, and S.-S. Li, arXiv:1201.1976.

[14] C.-H. Lee and C.-K. Yang, Phys. Rev. B **87**, 115306 (2013).

[15] C. K. Gaspe, S. Cairns, L. Lei, K. S. Wickramasinghe, T. D. Mishima, J. C. Keay, S. Q. Murphy, and M. B. Santos, J. Vac. Sci. Technol. B **31**, 03C129 (2013).

[16] S. Hikami, A. I. Larkin, and Y. Nagaoka, Prog. Theor. Phys. **63**, 707 (1980).

[17] B. L. Altshuler, A. G. Aronov, and D. E. Khmelnitsky, J. Phys. C: Solid State Phys. **15**, 7367 (1982).

[18] J. Chen, H. J. Qin, F. Yang, J. Liu, T. Guan, F. M. Qu, G. H. Zhang, J. R. Shi, X. C. Xie, C. L. Yang, K. H. Wu, Y. Q. Li, and L. Lu, Phys. Rev. Lett. **105**, 176602 (2010).

[19] J. Chen, X. Y. He, K. H. Wu, Z. Q. Ji, L. Lu, J. R. Shi, J. H. Smet, and Y. Q. Li, Phys. Rev. B **83**, 241304 (2011).

[20] Y. S. Kim, M. Brahlek, N. Bansal, E. Edrey, G. A. Kapilevich, K. Iida, M. Tanimura, Y. Horibe, S.-W. Cheong, and S. Oh, Phys. Rev. B **84**, 073109 (2011).

[21] M. Liu, C.-Z. Chang, Z. Zhang, Y. Zhang, W. Ruan, K. He, L.-l. Wang, X. Chen, J.-F. Jia, S.-C. Zhang, Q.-K. Xue, X. Ma, and Y. Wang, Phys. Rev. B **83**, 165440 (2011).

[22] H.-T. He, G. Wang, T. Zhang, I.-K. Sou, G. K. L. Wong, J.-N. Wang, H.-Z. Lu, S.-Q. Shen, and F.-C. Zhang, Phys. Rev. Lett. **106**, 166805 (2011).

[23] J. Wang, A. M. DaSilva, C.-Z. Chang, K. He, J. K. Jain, N. Samarth, X.-C. Ma, Q.-K. Xue, and M. H. W. Chan, Phys. Rev. B **83**, 245438 (2011).

[24] A. A. Taskin, S. Sasaki, K. Segawa, and Y. Ando, Phys. Rev. Lett. **109**, 066803 (2012).

[25] H. He, B. Li, H. Liu, X. Guo, Z. Wang, M. Xie, and J. Wang, Appl. Phys. Lett. **100**, 032105 (2012).

[26] N. Bansal, Y. S. Kim, M. Brahlek, E. Edrey, and S. Oh, Phys. Rev. Lett. **109**, 116804 (2012).

[27] M. M. Parish and P. B. Littlewood, Nature (London) **426**, 162 (2003).

[28] M. Büttiker, Phys. Rev. B **42**, 3197 (1990).

[29] C. M. Wang and X. L. Lei, Phys. Rev. B **86**, 035442 (2012).

[30] B. A. Assaf, T. Cardinal, P. Wei, F. Katmis, J. S. Moodera, and D. Heiman, Appl. Phys. Lett. **102**, 012102 (2013).

[31] H. Sakaki, T. Noda, K. Hirakawa, M. Tanaka, and T. Matsusue, Appl. Phys. Lett. **51**, 1934 (1987).

[32] W. Ning, F. Kong, C. Xi, D. Graf, H. Du, Y. Han, J. Yang, K. Yang, M. Tian, and Y. Zhang, ACS Nano **8**, 7506 (2014).